Electronic band structure of GaN diluted and overdiluted with group-V elements

Jakub Ziembicki,[*,¶] Rafał Bartoszewicz, Miłosz Grodzicki, Paweł Scharoch, and Robert Kudrawiec[†,‡]

Department of Semiconductor Materials Engineering, Wrocław University of Science and Technology, Wybrzeże Wyspiańskiego 27, 50-370 Wrocław, Poland

Wojciech Olszewski,[§,¶] Damian Pucicki,[‖] and Detlef Hommel

Łukasiewicz Research Network – PORT Polish Center for Technology Development, Stabłowicka 147, Wrocław 54-066, Poland

Maciej P. Polak

Department of Materials Science and Engineering, University of Wisconsin-Madison, 1509 University Ave., Madison, Wisconsin 53706, United States

(Received 18 August 2024; revised 18 November 2024; accepted 3 January 2025; published 3 February 2025)

The technology for manufacturing GaN-based devices is already very mature, but band engineering in this technology is still limited to mixing group-III elements, while the incorporation of group-V elements into GaN can create possibilities in band-gap engineering. In this work, we report comprehensive experimental studies of the electronic band structure for As-diluted and overdiluted GaNAs supported by computational methods based on the state-of-the-art density-functional-theory (DFT) approach. These studies clearly demonstrated that the incorporation of arsenic into GaN modifies the valence band, while the conduction band remains undisturbed up to 8% arsenic content. For the first time, As-related changes in the valence band are studied with high resolution in electron photoemission spectroscopy. As-related narrowing of the energy gap is also detected in the absorption spectra. These experimental observations are very consistent with the calculations of the electronic band structure for GaNAs, and therefore the same DFT approach was used to calculate the electronic band structure for GaN diluted and overdiluted with the remaining group-V elements, i.e., GaNP, GaNSb, and GaNBi. In this case, it is also clearly visible that adding P, Sb, or Bi to GaN modifies the valence band, while the conduction band remains undisturbed when the V-group concentration does not exceed 5%.

DOI: 10.1103/PhysRevApplied.23.024005

I. INTRODUCTION

Intensive research on group-III nitrides conducted over the last three decades has led to a breakthrough in lighting technology [1–3] and significant progress in the field of high-power transistors [4]. While this means that III-N technology is very mature, the band-gap engineering is still achieved only through mixing group-III elements, while, in general, in III-V semiconductors both groups, i.e., group III and V, can be mixed [5]. For zinc-blende III-V semiconductors such mixing is typical and various ternary (GaInAs, GaAsP, GaInSb, InAsSb), and quaternary (GaInPAs and GaInAsSb) alloys are widely used in light-emitting diodes, laser diodes, solar cells, and other semiconductor devices [6–8]. However, alloying group-III nitrides, which crystallize in the wurtzite (WZ) structure, with zinc-blende (ZB) III-V semiconductors is a significant technological challenge. This is related to a large lattice mismatch between these compounds as well as a large difference in the optimal growth temperature for these compounds [9]. Therefore, it is very difficult to obtain alloys of GaN with GaAs or GaSb over the full range of compositions in a crystalline phase [10–12]. It is, however, relatively easy to obtain ZB III-V alloys diluted with nitrogen [13,14]. Group-III nitrides diluted with a group-V elements (P, As, Sb, or Bi) are more difficult to synthesize, but significant progress in this field was achieved by molecular beam epitaxy (MBE) [10–12,15–19] or metal-organic vapor-phase epitaxy (MOVPE) [20–30]. Quite recently, it has been shown that the MOVPE method can be used to obtain crystalline GaNAs material with an arsenic content

[*]Contact author: jakub.ziembicki@pwr.edu.pl

[†]Contact author: robert.kudrawiec@pwr.edu.pl

[‡]Also at Łukasiewicz Research Network – PORT Polish Center for Technology Development, Stabłowicka 147, Wrocław 54-066, Poland.

[§]Also at Institute of Experimental Physics, University of Wrocław, pl. Maxa Borna 9, Wrocław 50-204, Poland.

[‖]Also at Department of Nanometrology, Faculty of Electronics, Photonics and Microsystems, Wrocław University of Science and Technology, 50-372 Wrocław, Poland.

[¶]These authors contributed equally.

of up to 7%, [31], which is well above the diluted regime (it is usually assumed that the diluted regime is up to 1–2%). For further development of III nitrides' technology, it is interesting and natural to explore the effect of the remaining group-V elements in the diluted regime and above it, even if it is still difficult from a technological point of view.

So far, interest in this type of semiconductor alloy has resulted from their unusual electronic properties, which are not present in regular III-V semiconductor alloys (GaInAs, GaPAs, or InAsSb). Therefore, this family of systems is recognized as separate and is called highly mismatched alloys (HMAs), which emphasizes their mismatch in the size (valence radii) of mixed group-V elements, as well as the difference in their electronegativity (i.e., nitrogen has a much smaller ionic radius and much greater electronegativity than the other group-V atoms). The electronic band structure for this type of alloy in the diluted regime can be described within the band anticrossing (BAC) model, [32,33] which was originally introduced for nitrogen-diluted Ga(In)NAs [32] and then extended to other nitrogen-diluted III-V semiconductors [34–37] as well as to III-N semiconductors diluted with group-V elements [9,38]. The BAC model is very convenient in predicting the dispersion of electronic bands, however its applicability is limited to the diluted regime and for higher concentration its predictions are not correct. The electronic band structure of HMAs has also been calculated from first principles, [39–44] but so far there are no papers on systematic calculations of the electronic structure for GaN with group V in the diluted regime and above.

Experimental studies of the electronic band structure for GaN diluted with group-V atoms are limited to determining the energy gap using absorption spectroscopy, [10,11,45] while it would be more informative to study changes in the valence band using photoelectron spectroscopy (PES) because this is where the main changes in the band structure are expected according to the BAC model [9,38]. In this case, ultraviolet excitation [i.e., ultraviolet photoelectron spectroscopy (UPS)], will be particularly interesting because it allows the examination of the density of valence-band states with greater accuracy than standard PES with x-ray excitation [i.e., x-ray photoelectron spectroscopy (XPS)]. However, so far this method has not been used to study GaN diluted with group-V elements. This means that changes in the valence band caused by these elements have not yet been properly investigated and experimentally confirmed.

This paper presents a comprehensive and systematic study of the electronic band structure for GaNAs with arsenic content up to 8%, both using experimental methods, i.e., UPS and absorption spectroscopy, and computational methods based on the state-of-the-art density-functional-theory (DFT) approach. Comparison of the DFT results with the experimental results allows us to discuss the applicability regime of the BAC model, its assumptions, and also allows us to perform a reliable analysis of the electronic band structure for GaN diluted and overdiluted with the remaining group-V elements. The obtained results clearly show that these materials, i.e., GaN diluted and overdiluted with group-V elements, constitute a characteristic group of alloys, which in terms of electronic band structure differs substantially from common III-N alloys, i.e., AlGaN, AlInN, and GaInN.

II. RESULTS AND DISCUSSION

A. BAC model

According to the BAC model, the introduction of a small amount of arsenic (or another V-group element) into the GaN host can be described by introducing a resonant level associated with this element near the valence band (VB) of the host material, as shown in Fig. 1(a). The position of the resonant level can be determined experimentally for the ultradilute alloy because photoluminescence (PL) can be observed between the conduction band and the resonant level [9]. Figure 1(a) shows the positions of the P, As, Sb, and Bi resonant levels in GaN measured by PL [9] and derived in this work from DFT calculations (see the following sections for details). It is clear that with the increasing mass of atoms, resonant levels shift to higher energies.

The electronic band structure modeled within the BAC model for GaNAs diluted with As is sketched in Fig. 1(b). The interaction between As-related and VB states is modeled using the perturbation theory described by the following Hamiltonian:

$$\hat{H}_{\mathrm{BAC}} = \begin{pmatrix} E_{\mathrm{VB}}(k) & C_{\mathrm{AsVB}}\sqrt{x} \\ C_{\mathrm{AsVB}}\sqrt{x} & E_{\mathrm{As}} \end{pmatrix}, \tag{1}$$

where E_{As} is the energy of the As-related states relative to the VB also referred to as a resonant level, $E_{\mathrm{VB}}(k)$ is the energy dispersion of the VB of the GaN host, C_{AsVB} is a constant that describes the interaction between the As-related and VB states, and x is the fraction of substitutional As atoms in $GaN_{(1-x)}As_x$ alloy. According to previous work, [38] the As energy level is located 0.62 eV above the VB in GaN and the coupling parameter $C_{\mathrm{AsVB}} = 0.75$ eV is adopted for N-rich GaNAs. Due to the interaction between dispersionless As-related states with VB states, E_+ and E_- subbands are formed in the VB. Their dispersions are given by

$$E_{\pm} = \frac{1}{2}\left[E_{\mathrm{As}} + E_{\mathrm{VB}} \pm \sqrt{(E_{\mathrm{As}} - E_{\mathrm{VB}})^2 + 4C_{\mathrm{AsVB}}^2 x}\right] \tag{2}$$

and their wave functions are given by

$$\Psi_{\pm} = c_{\pm}\,|\mathrm{As}\rangle \mp c_{\mp}\,|\mathrm{VB}\rangle\,, \tag{3}$$

where c_+ and c_- are constants, which describe mixing between VB and As states. In this case, the character of E_+ band is dispersion-less As-like (similar to impurity states)

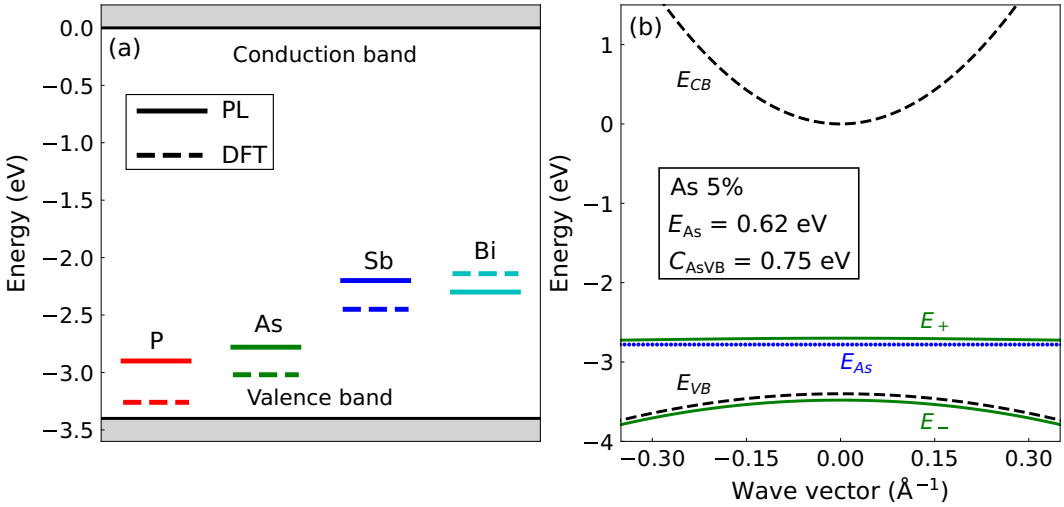

FIG. 1. (a) Resonant levels of group-V elements in GaN calculated in this work and taken from PL experiments [9]. (b) Band structure diagram of GaNAs described by the BAC model. The black dashed lines represent the band structure of the pure GaN host, while the blue dotted line denotes the E_{As} resonant level. The green lines indicate the band structure according to the BAC model, using parameters given in the frame [38].

while E_- is VB-like, i.e., similar to the VB in GaN host. According to the BAC model, the effect of As on the conduction band in arsenic-diluted GaNAs is neglected, as seen in Fig. 1(b).

Note that the BAC Hamiltonian is simplified, as the full Hamiltonian for the band-anticrossing interaction in the VB should be composed of three subbands typical of WZ GaN and three As-related states associated with the p_x, p_y, and p_z symmetry. However, for our purposes, the use of the simplified BAC Hamiltonian is sufficient, especially since the parameters for the full-valence BAC model are not well established. In the following sections, predictions of the BAC model will be compared to DFT calculations and experimental results.

B. DFT calculations

As mentioned in the Introduction, the BAC model is expected to work only in the diluted regime. Therefore, to obtain a more realistic picture of the electronic band structure for GaNAs diluted and overdiluted with arsenic, we used the state-of-the-art DFT methods. Figure 2 presents the effective band structure for gallium nitride with arsenic for concentrations ranging from 0% to 8%. For low arsenic concentrations, the band structure of GaNAs is very similar to that of the host material GaN, with the difference that additional bands appear above the valence band. The dispersion of these bands is negligible and they are very similar to the E_+ band in the BAC model, which is also nondispersive. On the other hand, the E_- band in the BAC

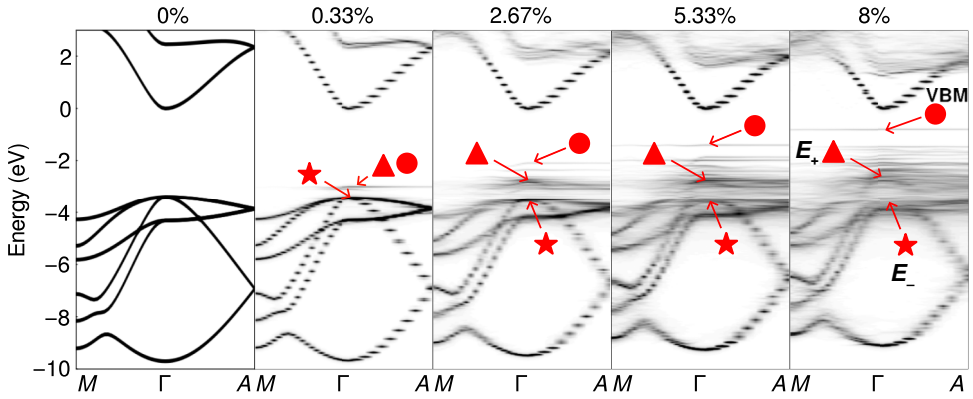

FIG. 2. Band structures of GaN diluted and overdiluted with As for different concentrations. E_+, E_-, and VBM are marked with red triangles, stars, and circles, respectively, and their energy is shown in Fig. 5. The conduction-band minimum in all band structures is set to zero energy.

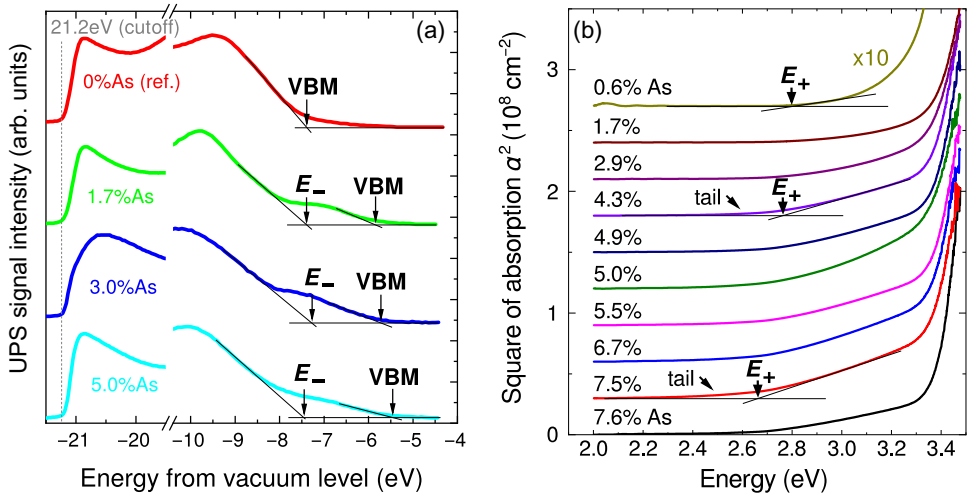

FIG. 3. UPS (a) and absorption (b) measurements of GaN with different As concentrations. Derived energy values of E_-, E_+, and VBM are marked with arrows and are shown on Fig. 5 as a function of As concentration.

model has a dispersion similar to the valence-band dispersion in GaN, and such a band can also be observed in the DFT calculations of the GaNAs band structure. These bands are symbolically marked in Fig. 2 by red triangles and stars. As the arsenic content increases, the intensity of bands (which correspond to their density of states) of E_+ states increases and it shifts slightly to higher energies. At high concentrations, an emergence of the parabolic dispersion can be observed at the location of the E_+ band for small wave vectors near the Γ point. At the same time, new states appear above E_+ with much lower density of states and significant spread in energy. The highest occupied state in the structure is marked in Fig. 2 by a red circle. In the next section, we confront these band structures with results of PES and absorption measurements.

The analysis of the first conductive band indicates that the effect of arsenic on this band is negligible, its dispersion remains the same as in pure GaN. Therefore, it is justified that As-related changes in the conduction band can be neglected in the BAC model. However, in the case of the next conduction band, it is clearly visible that as the arsenic content increases, this band broadens energetically and the distance between this band and the first conduction band decreases, see Fig. 2. This effect is due to the mixing of unoccupied *s* states of arsenic with the conduction bands of the host material.

C. Experiment

Figure 3 shows the UPS spectra scaled with an electron energy cutoff at −21.2 eV, which corresponds to the He I line. Thus, the energy at which the UPS signal appears corresponds to the position of the valence-band maximum (VBM) in GaNAs relative to the vacuum level. Additionally, a cutoff edge can be determined in the UPS spectra, which can be assigned to the E_- states in GaNAs, see Fig. 3. The position of this edge does not change much with increasing arsenic concentration in GaNAs, which is consistent with DFT calculations and the BAC model (see Fig. 5 for comparison). It is worthwhile to emphasize that so far the E_- edge has not been resolved in the PES spectra of GaNAs alloys. This may be related to the poorer spectral resolution in XPS, which has been used to study these alloys so far [31]. The spectral position of the states associated with the VBM is consistent with previous XPS studies for these crystals [31] (see Fig. 5).

Another experiment enabling the examination of the electronic band structure of GaN diluted and overdiluted with As was the measurement of absorption, which allows the determination of the optical energy gap and which has been used so far for this type of alloy [10,11,45]. Figure 3 shows the square of absorption α^2 for a set of GaNAs layers with different As concentrations in the spectral range of the absorption edges in this alloy. The strong absorption at 3.4 eV is related to the absorption edge in the GaN template, which is the substrate for the growth of GaNAs layers. Absorption in GaNAs layers appears below absorption in GaN. As the arsenic content in the GaNAs layers increases, this absorption increases and shifts slightly to lower energies. It is worth emphasizing here that for low As compositions, absorption occurs already at an energy of 2.8 eV. As the arsenic content increases, the absorption edge does not shift very significantly, which is consistent with previous studies [10,11,45] and the predictions of the BAC model in which the E_+ band is responsible for the absorption edge in GaNAs. This band appears immediately after the incorporation of a small amount of arsenic [45] and hence there is no continuous change in the energy gap from the GaN band gap to 2.8 eV.

The direct nature of the measured energy gap enables its determination on the basis of the relationship of absorption

coefficient and photon energy $\alpha(E)$:

$$\alpha(E) = \alpha_0 \sqrt{\frac{E - E_g}{E_g}}, \tag{4}$$

where E and E_g are the photon and band-gap energies, respectively. However, a clear determination of the absorption edge for GaNAs alloys is not so obvious because at low energy additional absorption with nonlinear character of α^2 and smaller intensity appears, see Fig. 3. Taking into account the valence-band structure resulting from DFT calculations (see Fig. 2), such absorption behavior is to be expected. Therefore, the linear part of the absorption spectrum is identified as the E_+ state, which in DFT calculations is assigned to most intensive states with emerging parabolic dispersion (red triangles in Fig. 2), whereas the tail after the linear part is due to states above E_+, which have much smaller intensities.

Figure 4 shows the evolution of the α_0 constant from Eq. (4) of both transitions mentioned in the previous paragraph with increasing concentration of arsenic. In the diluted regime, there is a significant increase of the absorption intensity, which then stabilizes and stays constant in the over-diluted regime. The values of α_0 are one order of magnitude smaller than in pure GaN in the whole range of concentrations. It is expected on the ground of previously shown DFT calculations, because the measured absorption is connected to states appearing above the host material valence band and these states have a density of states significantly smaller than the pure GaN valence band, which leads to smaller absorption.

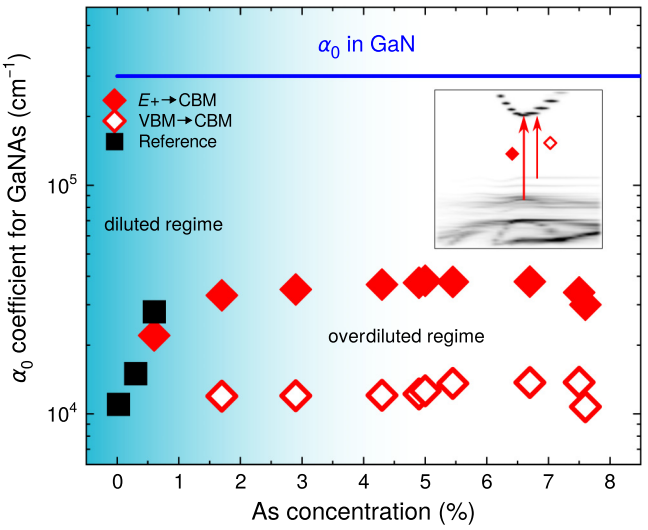

FIG. 4. α_0 constants for measured $E_+ \rightarrow$ CBM and VBM $\rightarrow$ CBM transitions as a function of arsenic concentration. Reference [45] in the diluted regime is also given. Inset: band structure of GaN diluted with As (2.67%), both measured transitions are marked with arrows.

In order to quantitatively compare the results of the measurements with DFT calculations and the predictions of the BAC model, the characteristic energies as a function of As concentration derived from all methods are plotted in Fig. 5. Following the BAC model, the energy of CBM is set to the same energy for all concentrations in both theoretical models. Then the overall picture is the following:

(1) Based on DFT band structures, three characteristic energies can be identified E_-, E_+, and VBM (see Fig. 2).
(2) BAC model predict E_- and E_+ energies with good agreement with DFT.
(3) XPS method resolves only the VBM, whereas UPS due to better resolution identifies also the E_- edge.
(4) Absorption measurements resolve the band gap associated with the $E_+ \rightarrow$ CBM transition, due to much higher DOS of E_+ compared to VBM, weak tail originating from states above E_+ can also be observed.

The above results are shown in Fig. 5 and a good quantitative agreement between the different methods is clearly visible. As the concentration of As goes to zero, the VBM and E_+ converge to the same energy. It is a diluted regime in which the BAC model correctly predicts the position of the VBM. On the other hand, with increasing concentration, the distance of VBM from E_+ increases significantly and the BAC model does not predict VBM correctly. In this overdiluted regime, the assumptions of the BAC model of isolated, noninteracting arsenic atoms are no longer correct and it has to be modified to include effects of interacting

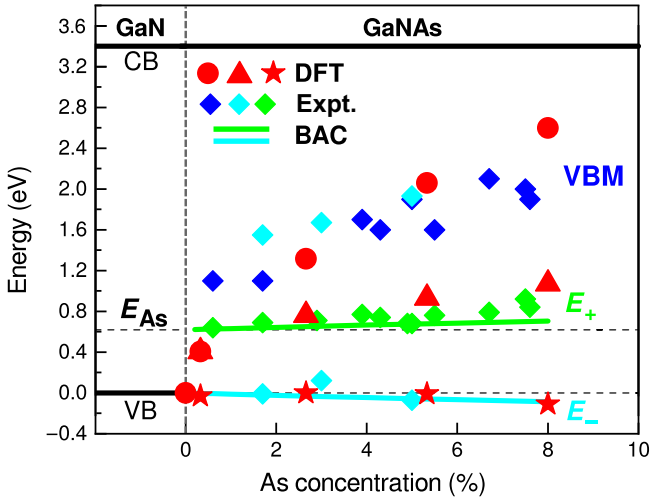

FIG. 5. Energy values of E_-, E_+, and VBM states derived from different methods: red markers are levels from DFT (see Fig. 2), blue markers are from XPS, [31] cyan markers are from UPS and green markers are from absorption (see Fig. 3). Solid green and cyan lines are predictions of the BAC model. Conduction-band minimum is set to the same energy for all As concentrations.

arsenic pairs and triplets. Remarkably, the predictions of this model are still in good agreement with absorption spectra even in the overdiluted regime, which indicates that even though the BAC model does not predict VBM correctly, it is still successful in predicting the region with the highest density of states, which dominates absorption spectra.

It is worth noting that the fundamental band gap determined from DFT for high concentrations is below 1.4 eV, which is the band-gap value for GaAs. Two points should be considered here. First, the band gap in HMA is typically measured by absorption, which yields an optical band gap higher than the fundamental band gap deduced from DFT, as discussed in the previous section. Second, the $GaN_{(1-x)}As_x$ band-gap dependence is expected to show strong nonlinearity, with a minimum occurring at some value of x. This is based on the behavior of its end components. In particular, it is known that in GaAs diluted with nitrogen, the band gap decreases with increasing nitrogen concentration, reaching values below 1 eV at x approaching approximately 0.96 [46].

D. Incorporation of other group-III and V elements into the GaN structure

The good agreement of DFT modeling with the experimental data encourages the exploration of GaN diluted and overdiluted with other group-III and V atoms. Starting with group V, Fig. 6 presents the effective band structures for gallium nitride diluted with phosphorus, arsenic, antimony, and bismuth for various concentration values. For low concentrations, a nondispersive state appears above the valence band, which for higher concentrations transforms into a whole family of states occupying a wide energy range. This can be interpreted as the emergence of the new band, especially considering the weak dispersion that can be observed at higher concentration. Generally, the energy distance of these states above the valence band and their energy broadening increase with concentration, and this effect is greater for heavier atoms. Consequently, the band gap is also significantly smaller for compounds with heavier atoms. On the other hand, dispersion of the first conduction band of host material remains unchanged, although for high concentrations some

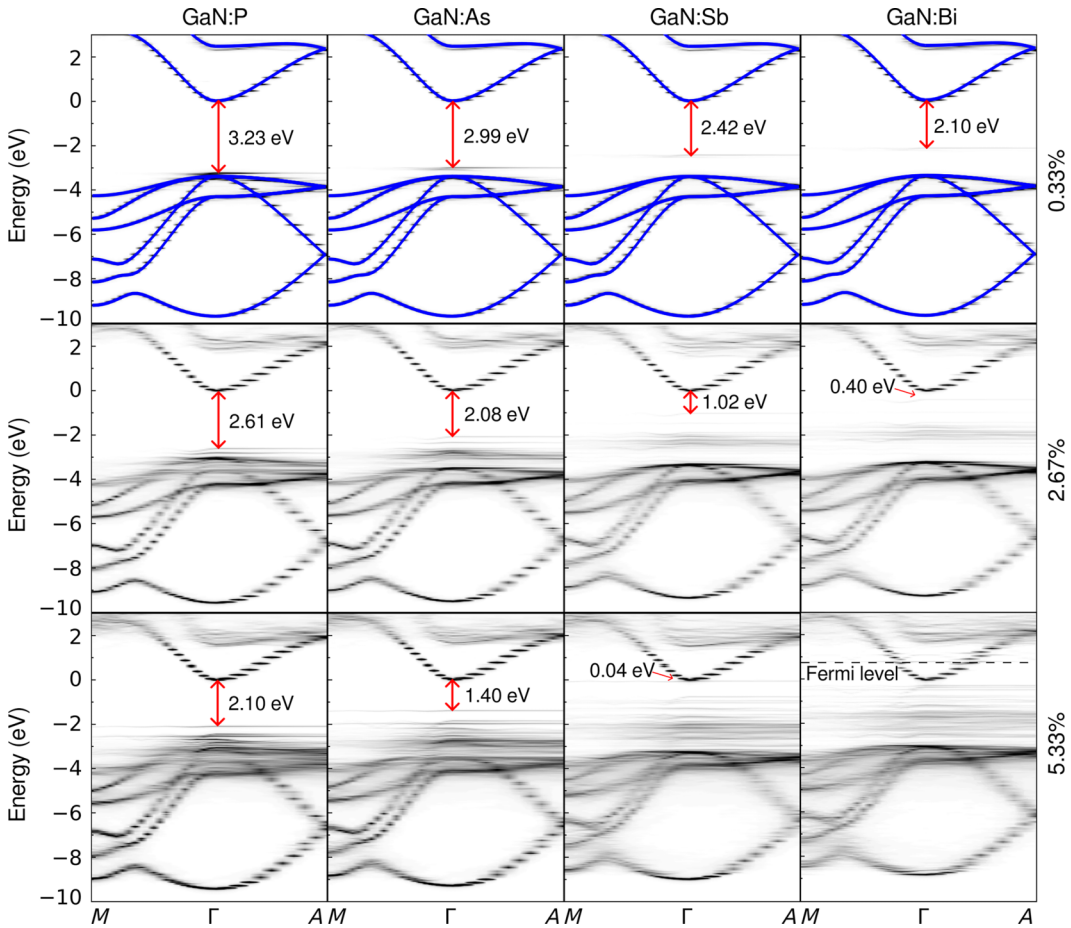

FIG. 6. Band structures of GaN diluted with P, As, Sb, and Bi. In the first row, the band structure of pure GaN is superimposed for comparison (blue lines). Fundamental band gaps are marked with red arrows and on the last graph with the metallic system, the Fermi level is marked.

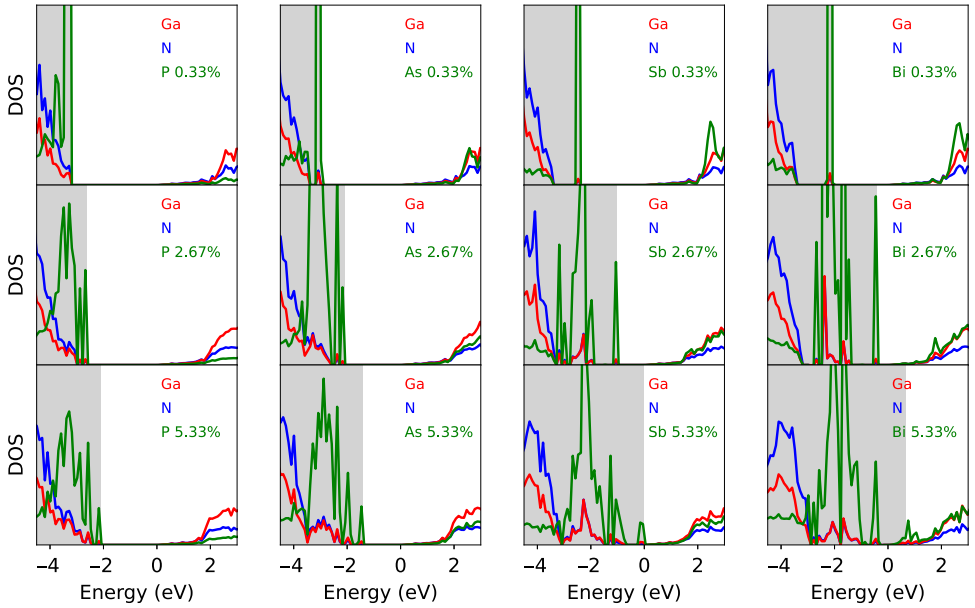

FIG. 7. Density of states of GaN diluted with P, As, Sb, and Bi. Occupied states are marked by gray background.

of the valence states start to overlap with CBM for GaNSb and GaNBi. At the same time, strong changes can be observed for the second conduction band, which broadens energetically and shifts closer to the first conduction band as the concentration increases. The resonant levels of group-V elements relative to the VBM of the host material derived from low concentration (0.33%) DFT band structures are equal to 0.14, 0.38, 0.95, and 1.26 eV for P, As, Sb, and Bi, respectively. These values are presented in Fig. 1 together with the values reported in previous studies [9]. Although there are some quantitative differences, the estimation of the resonant level from DFT and the experiment is not straightforward, as it depends on the concentration.

Figure 7 shows the density of states for the same structures, with the contribution from gallium, nitrogen, and the introduced group-V atom marked. DOS for every atom type is normalized by the number of atoms of that type in the supercell. These DOS structures confirm the above observations on the band structures, simultaneously indicating that the main contribution in the region of the band gap from the introduced group-V atoms lies precisely in these new states appearing above the GaN valence band. The energy broadening of these states with increasing concentration can also be clearly observed in Fig. 7. As mentioned earlier, the BAC model correctly predicts the position of the maximum in DOS originating from the introduced group-V element (at least in the case of GaNAs), but this maximum is the highest occupied state only in the diluted regime. Above this regime, they are states with significantly smaller DOS, located energetically above DOS maximum.

The situation is entirely different for the substitution of group-III atoms for gallium, as shown in Fig. 8. In this

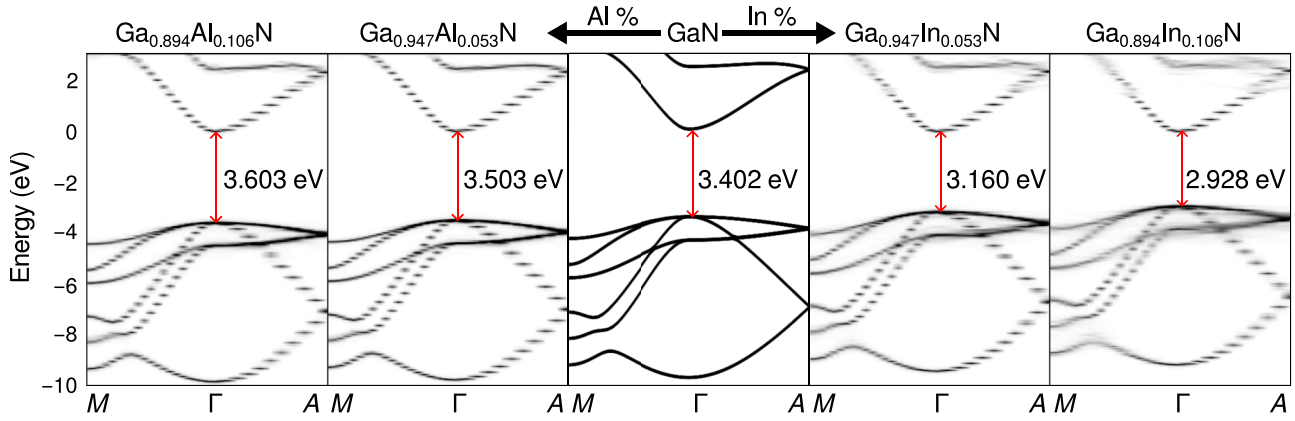

FIG. 8. Band structures of GaN diluted with Al and In. Band-gap values are marked with red arrows.

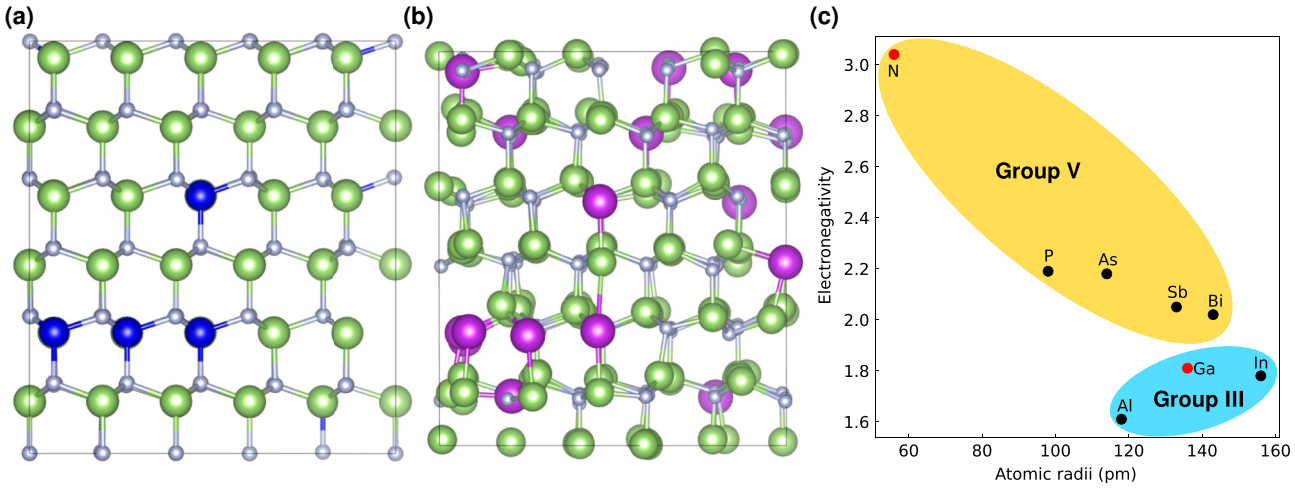

FIG. 9. Examples of supercells used for calculations with aluminium (a) and bismuth (b). In the case of bismuth, significant lattice distortion is observed. In (a),(b) green, gray, blue, and magenta balls indicate Ga, N, Al, and Bi, respectively. (c) Electronegativity of group-III and V elements as a function of atomic radii.

case, no new bands or significant broadening of the host GaN band structure can be observed. In contrast, for the studied compositions' range, very well-defined bulklike band structures can be observed and the main difference between different compositions is the continuous change in the band-gap value.

Understanding the differences between diluting gallium nitride with atoms of group III and group V can be found by looking at Fig. 9. It is immediately noticeable how the introduction of bismuth into the structure [Fig. 9(b)] introduces disorder in the system, significantly changing bond lengths and angles. This is completely opposite in the case of aluminium [Fig. 9(a)], which integrates into gallium positions without significant changes in the geometric structure. It is therefore not surprising that the introduction of bismuth leads to the appearance of nondispersive states, similar to defect states, because it introduces significant local lattice distortion, which in turn leads to an electronic configuration that does not occur in the pure GaN host material. Similar arguments can be applied to other atoms considered in this study.

This effect is intuitively simple to explain: aluminium, gallium, and indium atoms have similar radii and electronegativities, whereas nitrogen is much smaller and has a much higher electronegativity than the other group-V atoms [Fig. 9(c)]. In this sense, group-V atoms do not fit into the structure of GaN and introduce significant lattice distortion in their vicinity. Both these factors, i.e., electronegativity and radii differences contribute to the origin of states in the band gap, therefore it is interesting to study which one is more significant. We performed a simple test, where we calculated the band structure of GaNAs without optimization of atomic positions in supercell, so that all atoms were in their ideal positions. In that way, we excluded the effect of relaxation on the electronic structure. We observed that the calculated structures did not possess any states in the band gap, they resembled the GaN host band structure. Therefore, we claim that the main source of states in the band gap is a large difference in the atomic sizes of the group-V elements and the resulting lattice relaxations. Similar conclusions were drawn in previous work on the example of GaN diluted with P [47].

III. SUMMARY

In summary, systematic DFT studies of the electron band structure of GaN diluted and overdiluted with group-V elements have been carried out. The predictions were confronted with experimental results for the case of GaN diluted with As, namely UPS and absorption spectra. Theory and experiment clearly demonstrated that the incorporation of a diluted and overdiluted amount of group-V elements into GaN very significantly changes the electronic band structure in a valence-band region, leading to emergence of new states in the band gap. On the other hand, the first conduction band remains undisturbed when the group-V concentration does not exceed 5%. Such dramatic changes in the valence-band region are not observed when mixing with group-III elements, i.e., adding Al or In to GaN. Therefore, GaN diluted with group-V elements can be assigned to a separate class of alloys, namely highly mismatched alloys, with features not available in regular III-N alloys. The combination of regular III-N alloys with HMA opens up additional possibilities in band-gap engineering in GaN-based semiconductor devices, because of significant change in the band-gap values with small concentrations of added atoms and emergence of midgap

states. These features mark GaN HMA as promising candidates for light emitters and photodetectors in a broad spectrum range or high-efficiency hybrid solar cells.

IV. METHODS

GaNAs layers were grown in a vertical showerhead MOVPE reactor (CCS3x2FT AIXTRON) on sapphire substrates. A standard 2-μm-thick undoped GaN buffer layer was grown at 1045 °C before the GaNAs layer was deposited. Ammonia (NH_3), trimethylgallium (TMGa), and trimethylarsine (TMAs) were used as precursors and hydrogen as the carrier gas. Details on the growth parameters of GaNAs layers and their structural characterization are described in Ref. [31]

The ultraviolet photoelectron spectroscopy (UPS) and x-ray photoelectron spectroscopy (XPS) were performed with use of a hemispherical electron energy analyzer (Argus CU). Radiation sources for XPS and UPS were monochromatic Al Kα (1486.6 eV) and He I (21.22 eV), respectively. The step size of 0.05 eV and a pass energy of 20 eV were used for XPS analysis, and the step size of 0.01 eV and a pass energy of 1 eV were used for UPS. The experiment was performed at room temperature and a take-off angle of 60° with respect to the surface. Binding-energy values are calibrated to the Fermi level of the electron analyzer, the position of which was determined using a cleaned reference Ag sample.

To determine the absorption spectra of GaNAs layers, light transmission and reflectance measurements were performed. For this purpose, the samples were polished from the sapphire-substrate side. Transmission and reflectance measurements were performed using the lock-in technique with a halogen lamp, a 0.5-m monochromator (Zolix Omni-λ series), and a silicon diode.

All DFT calculations were performed using the VASP package and the PAW method [48–51]. For geometry optimization, the LDA functional was used [52,53], which accurately reproduces the experimental values of the lattice constants of GaN (a and c equal to 3.187 and 5.184 Å compared to experimental values of 3.189 and 5.185 Å) [46]. For band-structure calculations, the MBJ functional was used [54], which gives an energy gap for GaN (3.402 eV) consistent with the experiment (3.44 eV) [46]. A cutoff energy of 600 eV and a Brillouin-zone sampling grid of $2 \times 2 \times 2$ were used for the calculations of the mixed compound supercells. In the optimized geometric structures, all forces in the system were below 0.05 eV/Å.

For the simulation of the mixed compound, a supercell approach was used [47]. A supercell consisting of a $5 \times 5 \times 3$ multiplication of the primitive unit cell of GaN was used, containing 300 atoms in total. Subsequently, either random nitrogen atoms were substituted by phosphorus, arsenic, antimony, or bismuth atoms or random gallium atoms were substituted by aluminium and indium atoms. The substitution was carried out according to the special quasirandom structure (SQS) procedure [55] as implemented in the ATAT code [56]. The SQS approach allows for the generation of a supercell that best approximates an ideally disordered system [55]. To generate the supercell, correlations for two-atom clusters smaller than 6.4 Å and three-atom clusters smaller than 5.2 Å were checked. The structure was searched with the MCSQS code until no better structure was found for several hours. Then the atomic positions and lattice constants in the obtained supercells were optimized using the VASP package. An example of supercells with aluminium and bismuth atoms are shown in Fig. 9. In order to get the effective band structure of random alloy, the unfolding procedure [47] was carried out by means of VaspBandUnfolding code [57].

ACKNOWLEDGMENTS

This work was funded within the Grants of the National Science Center Poland (No. OPUS15 2018/29/B/ST3/02731) and (No. PRELUDIUM21 2022/45/N/ST5/03912). Calculations have been carried out using resources provided by the Wroclaw Centre for Networking and Supercomputing.

DATA AVAILABILITY

The data that support the findings of this article are openly available [1].

[1] I. Akasaki, Nobel lecture: Fascinated journeys into blue light, Rev. Mod. Phys. **87**, 1119 (2015).
[2] H. Amano, Nobel lecture: Growth of GaN on sapphire via low-temperature deposited buffer layer and realization of p-type GaN by Mg doping followed by low-energy electron beam irradiation, Rev. Mod. Phys. **87**, 1133 (2015).
[3] S. Nakamura, Nobel lecture: Background story of the invention of efficient blue InGaN light emitting diodes, Rev. Mod. Phys. **87**, 1139 (2015).
[4] M. H. Wong, S. Keller, S.D. Nidhi, J. Denninghoff, S. Kolluri, D. F. Brown, J. Lu, N. A. Fichtenbaum, E. Ahmadi, E. Singisetti, *et al.*, N-polar GaN epitaxy and high electron mobility transistors, Semicond. Sci. Technol. **28**, 074009 (2013).
[5] I. Vurgaftman, J. R. Meyer, and L. R. Ram-Mohan, Band parameters for III–V compound semiconductors and their alloys, J. Appl. Phys. **89**, 5815 (2001).
[6] Z. Yin and X. Tang, A review of energy bandgap engineering in III–V semiconductor alloys for mid-infrared laser applications, Solid State Electron. **51**, 6 (2007).
[7] A. E. Yachmenev, S. S. Pushkarev, R. R. Reznik, R. A. Khabibullin, and D. S. Ponomarev, Arsenides- and related III-V materials-based multilayered structures for terahertz applications: Various designs and growth technology, Prog. Cryst. Growth Charact. Mater. **66**, 100485 (2020).

[8] J. Li, A. Aierken, Y. Liu, Y. Zhuang, X. Yang, J. H. Mo, R. K. Fan, Q. Y. Chen, S. Y. Zhang, Y. M. Huang, *et al.*, A brief review of high efficiency III-V solar cells for space application, Front. Phys. **8**, 631925 (2021).

[9] R. Kudrawiec and D. Hommel, Bandgap engineering in III-nitrides with boron and group V elements: Toward applications in ultraviolet emitters, Appl. Phys. Rev. **7**, 041314 (2020).

[10] K. M. Yu, S. V. Novikov, R. Broesler, I. N. Demchenko, J. D. Denlinger, Z. Liliental-Weber, F. Luckert, R. W. Martin, W. Walukiewicz, and C. T. Foxon, Highly mismatched crystalline and amorphous $GaN_{1-x}As_x$ alloys in the whole composition range, J. Appl. Phys. **106**, 103709 (2009).

[11] S. Novikov, C. Staddon, C. Foxon, K. Yu, R. Broesler, M. Hawkridge, Z. Liliental-Weber, J. Denlinger, I. Demchenko, F. Luckert, *et al.*, Growth by molecular beam epitaxy of amorphous and crystalline GaNAs alloys with band gaps from 3.4 to 0.8 eV for solar energy conversion devices, J. Cryst. Growth **323**, 60 (2011).

[12] K. M. Yu, S. V. Novikov, M. Ting, W. L. Sarney, S. P. Svensson, M. Shaw, R. W. Martin, W. Walukiewicz, and C. T. Foxon, Growth and characterization of highly mismatched $GaN_{1-x}Sb_x$ alloys, J. Appl. Phys. **116**, 123704 (2014).

[13] M. Henini, *Dilute Nitride Semiconductors* (Elsevier, Amsterdam, Netherlands, 2005).

[14] J. S. Harris, R. Kudrawiec, H. B. Yuen, S. R. Bank, H. P. Bae, M. A. Wistey, D. Jackrel, E. R. Pickett, T. Sarmiento, L. L. Goddard, *et al.*, Development of GaInNAsSb alloys: Growth, band structure, optical properties and applications, Phys. Status Solidi (b) **244**, 2707 (2007).

[15] T.-Y. Seong, I.-T. Bae, C.-J. Choi, D. Y. Noh, Y. Zhao, and C. W. Tu, Microstructures of $GaN_{1-x}P_x$ layers grown on (0001) GaN substrates by gas source molecular beam epitaxy, J. Appl. Phys. **85**, 3192 (1999).

[16] C. Foxon, S. Novikov, T. Li, R. Campion, A. Winser, I. Harrison, M. Kappers, and C. Humphreys, Arsenic incorporation in GaN during growth by molecular beam epitaxy, J. Cryst. Growth **251**, 510 (2003).

[17] S. V. Novikov, K. M. Yu, A. X. Levander, Z. Liliental-Weber, R. dos Reis, A. J. Kent, A. Tseng, O. D. Dubon, J. Wu, J. Denlinger, *et al.*, Molecular beam epitaxy of $GaN_{1-x}Bi_x$ alloys with high bismuth content, Phys. Status Solidi (a) **209**, 419 (2012).

[18] K. M. Yu, W. L. Sarney, S. V. Novikov, D. Detert, R. Zhao, J. D. Denlinger, S. P. Svensson, O. D. Dubon, W. Walukiewicz, and C. T. Foxon, Highly mismatched N-rich $GaN_{1-x}Sb_x$ films grown by low temperature molecular beam epitaxy, Appl. Phys. Lett. **102**, 102104 (2013).

[19] K. M. Yu, W. L. Sarney, S. V. Novikov, N. Segercrantz, M. Ting, M. Shaw, S. P. Svensson, R. W. Martin, W. Walukiewicz, and C. T. Foxon, Highly mismatched $GaN_{1-x}Sb_x$ alloys: Synthesis, structure and electronic properties, Semicond. Sci. Technol. **31**, 083001 (2016).

[20] S. Yoshida, J. Kikawa, and Y. Itoh, Crystal growth of nitride-rich GaNP by laser-assisted metalorganic chemical-vapor deposition, J. Cryst. Growth **237–239**, 1037 (2002).

[21] D. Chen, B. Shen, Z. Bi, K. Zhang, S. Gu, R. Zhang, Y. Shi, Y. Zheng, X. Sun, S. Wan, *et al.*, $GaN_{1-x}P_x$ ternary alloys with high P composition grown by metal-organic chemical vapor deposition, J. Cryst. Growth **255**, 52 (2003).

[22] Y. Tsuda, H. Mouri, M. Araki, Y. Ueta, T. Yuasa, and M. Taneya, Characterization of the GaN-rich side of GaNP grown by metal-organic chemical vapor deposition, Phys. Status Solidi (b) **240**, 404 (2003).

[23] D. Chen, B. Shen, Z. Bi, K. Zhang, S. Gu, R. Zhang, Y. Shi, and Y. Zheng, Characterization of $GaN_{1-x}P_x$ alloys grown by metal-organic chemical vapor deposition, Opt. Mater. **23**, 127 (2003).

[24] H. J. Kim, T. G. Andersson, J.-M. Chauveau, and A. Trampert, Arsenic incorporation and its influence on microstructure of wurtzite GaN grown by molecular-beam epitaxy, J. Appl. Phys. **94**, 7193 (2003).

[25] H. Na, H. J. Kim, E. Yoon, C. Sone, and Y. Park, Arsenic incorporation and growth mode of GaNAs grown by low-pressure metal-organic chemical vapor deposition, J. Cryst. Growth **248**, 437 (2003).

[26] H. D. Li, M. Tsukihara, Y. Naoi, Y. B. Lee, and S. Sakai, Investigations of V-shaped defects and photoluminescence of thin GaN-rich GaNP layers grown on a GaN epilayer by metalorganic chemical vapor deposition, Appl. Phys. Lett. **84**, 1886 (2004).

[27] A. Kimura, C. A. Paulson, H. F. Tang, and T. F. Kuech, Epitaxial $GaN_{1-y}As_y$ layers with high As content grown by metalorganic vapor phase epitaxy and their band gap energy, Appl. Phys. Lett. **84**, 1489 (2004).

[28] S.-H. Moon, H.-A. Do, J. Park, and S.-W. Ryu, Strong below-band gap absorption of N-rich side GaNSb by metal-organic chemical vapor deposition, J. Mater. Res. **24**, 3569 (2009).

[29] S. Sunkara, V. K. Vendra, J. B. Jasinski, T. Deutsch, A. N. Andriotis, K. Rajan, M. Menon, and M. Sunkara, New visible light absorbing materials for solar fuels, $Ga(Sb_x)N_{1-x}$, Advanced Materials **26**, 2878 (2014).

[30] D. Komori, K. Takarabe, T. Takeuchi, T. Miyajima, S. Kamiyama, M. Iwaya, and I. Akasaki, GaNSb alloys grown with H_2 and N_2 carrier gases, Jpn. J. Appl. Phys. **55**, 05FD01 (2016).

[31] W. Olszewski, D. Majchrzak, M. Grodzicki, J. Serafińczuk, S. Gorantla, D. Pucicki, P. P. Michałowski, R. Kudrawiec, and D. Hommel, Monocrystalline GaN diluted with up to 7% arsenic grown by MOVPE, Cryst. Growth Des. **24**, 4057 (2024).

[32] W. Shan, W. Walukiewicz, J. W. Ager, E. E. Haller, J. F. Geisz, D. J. Friedman, J. M. Olson, and S. R. Kurtz, Band anticrossing in GaInNAs alloys, Phys. Rev. Lett. **82**, 1221 (1999).

[33] J. Wu, W. Shan, and W. Walukiewicz, Band anticrossing in highly mismatched III-V semiconductor alloys, Semicond. Sci. Technol. **17**, 860 (2002).

[34] I. A. Buyanova, M. Izadifard, A. Kasic, H. Arwin, W. M. Chen, H. P. Xin, Y. G. Hong, and C. W. Tu, Analysis of band anticrossing in GaN_xP_{1-x} alloys, Phys. Rev. B **70**, 085209 (2004).

[35] T. D. Veal, L. F. J. Piper, P. H. Jefferson, I. Mahboob, C. F. McConville, M. Merrick, T. J. C. Hosea, B. N. Murdin, and M. Hopkinson, Photoluminescence spectroscopy of bandgap reduction in dilute InNAs alloys, Appl. Phys. Lett. **87**, 182114 (2005).

[36] P. H. Jefferson, T. D. Veal, L. F. J. Piper, B. R. Bennett, C. F. McConville, B. N. Murdin, L. Buckle, G. W. Smith, and T. Ashley, Band anticrossing in GaN_xSb_{1-x}, Appl. Phys. Lett. **89**, 111921 (2006).

[37] R. Kudrawiec, A. V. Luce, M. Gladysiewicz, M. Ting, Y. J. Kuang, C. W. Tu, O. D. Dubon, K. M. Yu, and W. Walukiewicz, Electronic band structure of $GaN_xP_yAs_{1-x-y}$ highly mismatched alloys: Suitability for intermediate-band solar cells, Phys. Rev. Appl. **1**, 034007 (2014).

[38] J. Wu, W. Walukiewicz, K. M. Yu, J. D. Denlinger, W. Shan, J. W. Ager, A. Kimura, H. F. Tang, and T. F. Kuech, Valence band hybridization in N-rich $GaN_{1-x}As_x$ alloys, Phys. Rev. B **70**, 115214 (2004).

[39] P. R. C. Kent and A. Zunger, Theory of electronic structure evolution in GaAsN and GaPN alloys, Phys. Rev. B **64**, 115208 (2001).

[40] P. R. Kent, L. Bellaiche, and A. Zunger, Pseudopotential theory of dilute III-V nitrides, Semicond. Sci. Technol. **17**, 851 (2002).

[41] D. Borovac, C.-K. Tan, and N. Tansu, First-principle study of the optical properties of dilute-P $GaN_{1-x}P_x$ alloys, Sci. Rep. **8**, 6025 (2018).

[42] J. C. Goodrich, D. Borovac, C.-K. Tan, and N. Tansu, Band anti-crossing model in dilute-As GaNAs alloys, Sci. Rep. **9**, 5128 (2019).

[43] M. P. Polak, R. Kudrawiec, and O. Rubel, Electronic band structure of nitrogen diluted Ga(PAsN): Formation of the intermediate band, direct and indirect optical transitions, and localization of states, J. Appl. Phys. **126**, 175701 (2019).

[44] M. P. Polak, P. Scharoch, and R. Kudrawiec, The effect of isovalent doping on the electronic band structure of group IV semiconductors, J. Phys. D: Appl. Phys. **54**, 085102 (2020).

[45] E. Zdanowicz, P. Ciechanowicz, K. Opolczynska, D. Majchrzak, J.-G. Rousset, E. Piskorska-Hommel, M. Grodzicki, K. Komorowska, J. Serafinczuk, D. Hommel, and R. Kudrawiec, As-related stability of the band gap temperature dependence in N-rich GaNAs, Appl. Phys. Lett. **115**, 092106 (2019).

[46] I. Vurgaftman and J. R. Meyer, Band parameters for nitrogen-containing semiconductors, J. Appl. Phys. **94**, 3675 (2003).

[47] V. Popescu and A. Zunger, Extracting E versus k effective band structure from supercell calculations on alloys and impurities, Phys. Rev. B **85**, 085201 (2012).

[48] G. Kresse and J. Hafner, Ab initio molecular dynamics for liquid metals, Phys. Rev. B **47**, 558 (1993).

[49] G. Kresse and J. Furthmüller, Efficient iterative schemes for ab initio total-energy calculations using a plane-wave basis set, Phys. Rev. B **54**, 11169 (1996).

[50] G. Kresse and J. Furthmüller, Efficiency of ab-initio total energy calculations for metals and semiconductors using a plane-wave basis set, Comput. Mater. Sci. **6**, 15 (1996).

[51] G. Kresse and D. Joubert, From ultrasoft pseudopotentials to the projector augmented-wave method, Phys. Rev. B **59**, 1758 (1999).

[52] D. M. Ceperley and B. J. Alder, Ground state of the electron gas by a stochastic method, Phys. Rev. Lett. **45**, 566 (1980).

[53] J. P. Perdew and A. Zunger, Self-interaction correction to density-functional approximations for many-electron systems, Phys. Rev. B **23**, 5048 (1981).

[54] F. Tran and P. Blaha, Accurate band gaps of semiconductors and insulators with a semilocal exchange-correlation potential, Phys. Rev. Lett. **102**, 226401 (2009).

[55] A. van de Walle, P. Tiwary, M. de Jong, D. Olmsted, M. Asta, A. Dick, D. Shin, Y. Wang, L.-Q. Chen, and Z.-K. Liu, Efficient stochastic generation of special quasirandom structures, Calphad **42**, 13 (2013).

[56] A. van de Walle, M. Asta, and G. Ceder, The alloy theoretic automated toolkit: A user guide, Calphad **26**, 539 (2002).

[57] Q. Zheng, VaspBandUnfolding, https://github.com/QijingZheng/VaspBandUnfolding.